A Wideband Microwave Double-Negative Metamaterial with Non-Foster Loading

Thomas P. Weldon, Konrad Miehle, Ryan S. Adams, and Kasra Daneshvar
Department of Electrical and Computer Engineering
University of North Carolina at Charlotte
Charlotte, NC 28223, USA
Email: tpweldon@uncc.edu

***Abstract*—Although the potential for wideband double-negative metamaterials using non-Foster circuit elements was described more than a decade ago, progress has been somewhat limited. Therefore, the analysis and simulation of a wideband microwave metamaterial are presented, where non-Foster elements are used as loads on split rings and on electric resonators. Using the Faraday law of induction, load conditions are derived for wideband negative permeability of a split ring. Using the Ampere circuital law, load conditions are derived for wideband negative permittivity of an electric resonator comprised of two disks connected by a rod. Simulations and extracted parameters confirm the underlying theory, and a wideband double-negative behavior is observed from 1.0 to 4.5 GHz for the proposed design.**

I. Introduction

Metamaterials offer tremendous potential in a wide range of applications such as negative refraction, flat lenses, and cloaking [1]–[5]. Although there has been considerable progress in passive metamaterials, the bandwidth of these devices remains limited by the resonant behavior of the fundamental particles or unit cells comprising the metamaterial. In contrast, non-Foster circuit elements offer the possibility of achieving performance capabilities well beyond the reach of passive components. Although the theoretical potential for non-Foster elements to increase the bandwidth of negative-index metamaterials is well known, limited progress has been made in this area [6]. Recently, Hrabar *et al.* demonstrated non-Foster circuits in a split-ring resonator [7]. In addition, Kim *et al.*, use shorted stubs on waveguides to achieve negative permeability and posts inside the waveguide to produce negative permittivity [8]. However, a complete wideband double-negative metamaterial design has remained somewhat elusive.

To address these issues, a wideband double-negative metamaterial is proposed having simultaneous negative permittivity and negative permeability from 1.0 to 4.5 GHz. To achieve this, non-Foster loads are added to a single-split-ring resonator (SSRR) and to an electric disk resonator (EDR) comprised of two metal disks connected by a metal rod [9]. The design of the loads for the SSRR and EDR that comprise the unit cell are based on analysis of the coupled fields. The required negative inductance load of the SSRR is derived using Faraday's law of induction and the incident magnetic field. The required negative capacitance load of the EDR is derived using Ampere's circuital and the incident electric field. The results from Faraday's law and Ampere's law are then used to compute the magnetic and electric dipole moments of the unit cell and to derive effective permittivity and permeability [10]. This straightforward analysis leads to a simple expression for the resulting negative effective permittivity and negative effective permeability of the unit cell as a function of frequency, with elimination of typical resonant behavior [1]. Thus, the proposed approach provides more direct insight into the interaction of the device with the electromagnetic field than may be offered by circuit-based approaches or models [11].

The following results and analyses address the problem of narrow bandwidth in double-negative metamaterials. In this, properly chosen non-Foster loads are shown to provide wideband negative effective permittivity, wideband negative effective permeability, and wideband double-negative metamaterials. In particular, the permeability of an SSRR becomes independent of frequency with a negative inductance load, and the permittivity of an EDR becomes independent of frequency with a negative capacitor load. Similar results for loop and dipole antennas were noted in [6].

In the following section, the design of a non-Foster-loaded SSRR with wideband negative permeability is first considered. The subsequent section considers the design of a non-Foster-loaded EDR with wideband negative permittivity. Finally, simulation results of wideband double-negative metamaterials are given, with effective permittivity and permeability extracted from the S-parameters of the metamaterial.

II. Wideband Negative Permeability Analysis

The well-known theory of an elementary lossless split ring resonator is first considered, since it will be useful in describing the overall analysis approach for the proposed negative-permittivity metamaterials in the following section [1], [12]. Although other resonators may have advantages, they would unnecessarily complicate the basic development outlined here.

Consider the single-split-ring resonator (SSRR) in Fig. 1 that is expected to exhibit a typical narrowband resonant behavior. The dimensions of the unit cell comprising this magnetic metamaterial particle are l_x, l_y, and l_z, and the split ring has an area A_R. As usual, the dimensions of the unit cell are considered significantly smaller than a wavelength. The incident magnetic field $H_\circ\hat{\mathbf{x}}$ is parallel to the axis of the ring.

As shown in Fig. 1, the current in the split ring is defined as i_r, and the voltage across the gap is v_g. (This sign

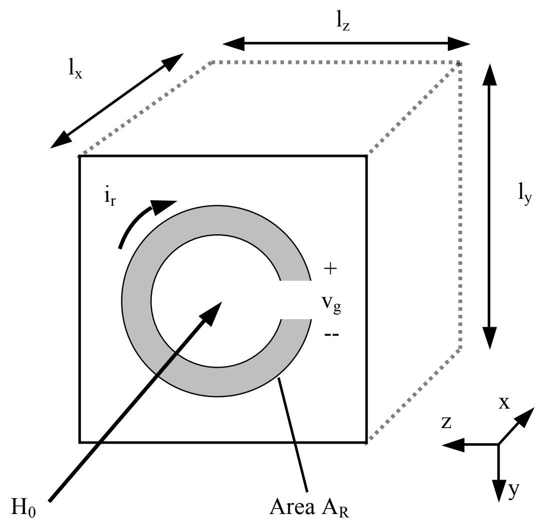

Fig. 1. Magnetic unit cell example showing single-split-ring resonator (SSRR).

convention for i_r and v_g is later convenient for describing the current through the capacitance of the gap in the ring.) Using Faraday's law of induction, the gap voltage is

$$v_g = -\frac{d\Phi_T}{dt} = -\frac{d\left(\Phi_0 + \Phi_R\right)}{dt} \ , \tag{1}$$

where Φ_T is the total magnetic flux in the SSRR, $\Phi_0 = \mu_\circ H_0 A_R$ is the incident magnetic flux over the split ring, A_R is the area of the SSRR, and Φ_R is the magnetic flux due to i_r. Then, the current in the ring is

$$i_r = C_g \frac{dv_g}{dt} = -C_g \frac{d^2\left(\Phi_0 + \Phi_R\right)}{dt^2} \ , \tag{2}$$

where C_g is the total capacitance across the gap of the SSRR. Taking the Laplace transform:

$$i_r = -s^2 C_g \left(\Phi_0 + \Phi_R\right) = -s^2 C_g \left(\Phi_0 + L_R i_r\right) \ , \tag{3}$$

where the self-inductance of the SSRR is $L_R = \Phi_R / i_r$. Solving for i_r yields the frequency-dependent current

$$i_r = -\Phi_0 \ \frac{s^2 C_g}{1 + s^2 L_R C_g} \ . \tag{4}$$

Next, consider replacing the gap capacitance C_g with a positive inductance L_g with reactance $X_g = j\omega L_g$. The voltage v_g now appears across this gap inductance L_g. Then, the current in the ring becomes

$$i_r = \frac{1}{L_g} \int v_g \, dt = -\frac{1}{L_g} \int \frac{d\left(\Phi_0 + \Phi_R\right)}{dt} dt \ . \tag{5}$$

after substituting for v_g from (1). Taking the integral, and again with $L_R = \Phi_R / i_r$, leads to

$$i_r = -\frac{1}{L_g} \left(\Phi_0 + \Phi_R\right) = -\frac{1}{L_g} \left(\Phi_0 + L_R i_r\right) \ . \tag{6}$$

Then, solving for i_r results in

$$i_r = -\Phi_0 \frac{1}{L_g + L_R} \ . \tag{7}$$

Comparing (7) with (4), the ring current i_r in (7) *no longer depends on frequency* when the gap capacitance C_g is replaced by inductance L_g, allowing wideband behavior.

The current in the loop gives rise to a magnetic dipole moment in the SSRR of $\mathbf{m} = i_r A_r \hat{\mathbf{x}}$. The minus sign in (7) then results in $\mathbf{m}$ having a direction opposite to the applied field $H_\circ \hat{\mathbf{x}}$. The macroscopic magnetization $\mathbf{M}$ is then the magnetic dipole moment per unit volume:

$$\mathbf{M} = -\ \Phi_0 \frac{A_R}{l_x l_y l_z} \frac{1}{L_g + L_R} \, \hat{\mathbf{x}} = -\ \mu_0 H_0 \frac{A_R^2}{l_x l_y l_z} \frac{1}{L_g + L_R} \, \hat{\mathbf{x}}. \tag{8}$$

where the permeability of free space is $\mu_\circ = 1.26 \times 10^{-6}$ H/m, and for simplicity omitting mixing effects noted in [13]. With $\mathbf{M} = \chi_m \mathbf{H}$ and $\mu_r = 1 + \chi_m$, it follows that

$$\mu_r = 1 - \mu_\circ \frac{A_R^2}{l_x l_y l_z} \ \frac{1}{L_g + L_R} \ . \tag{9}$$

where χ_m is the magnetic susceptibility, and μ_r is the effective relative permeability of the metamaterial.

The proposed effective relative permeability μ_r for the SSRR given in (9) does not vary with frequency and becomes a large negative value if L_g is chosen to be negative such that the denominator has $(L_g + L_R) > 0$ and $(L_g + L_R) \approx 0$. *Thus, a negative inductor load in the gap of a SSRR can provide wideband negative effective permeability.* The desired condition $(L_g + L_R) > 0$ has the same form as a series combination of a negative inductor with a positive inductor whose resulting inductance remains positive [14]. Non-Foster circuits such as a negative inductor can be designed using negative impedance converters, where recent progress has been made in potential stability issues [14], [15].

III. Wideband Negative Permittivity Analysis

Just as the theory of the SSRR was developed above for wideband negative-permeability metamaterials, a similar approach is now used to develop the theory for the proposed wideband negative-permittivity metamaterials. The analysis follows along similar lines as the analysis of the magnetic unit cell of Fig. 1 [9].

Consider the electric disk resonator (EDR) in Fig. 2, resembling a three-dimensional version of the I-shaped structures in [10] and [16]. The dimensions of the unit cell comprising this electric metamaterial particle are the same as the magnetic component of Fig. 1, l_x, l_y, and l_z. The metal disks near the top and bottom faces of the structure have areas A_D, and are connected together by a metal post with inductance L_p. As usual, the dimensions of the unit cell are taken to be less than a wavelength, so that the incident electric field $E_0 \hat{\mathbf{y}}$ is uniform over the unit cell. As shown in Fig. 2, the current in the post that connects the two disks is i_p, and the voltage between the upper and lower disk is v_d.

Using Ampere's circuital law and the Maxwell-Ampere equation, the time derivative of the total electric flux impinging

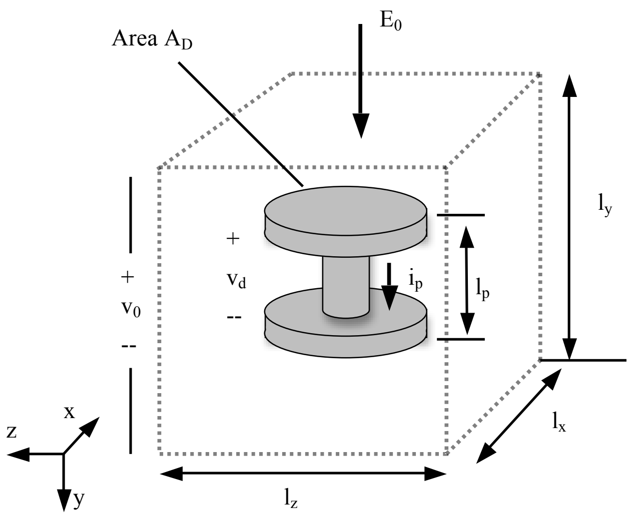

Fig. 2. Electric unit cell example showing electric disk resonator (EDR) comprised of two metal disks connected by a cylindrical metal post of length l_p with inductance L_p.

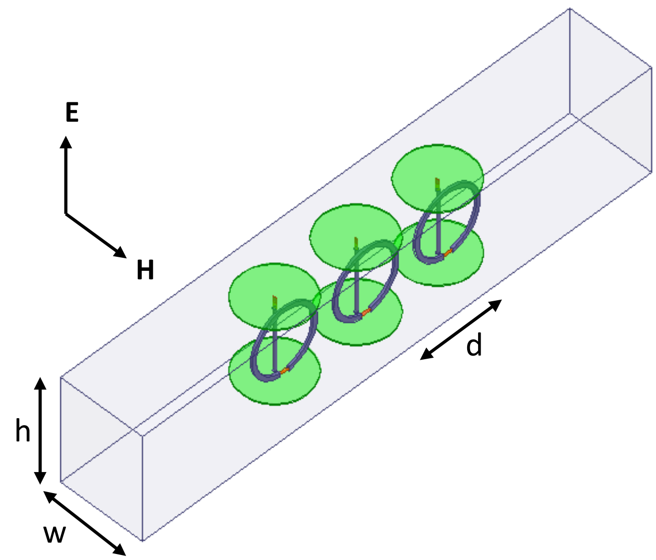

Fig. 3. Double-negative structure consisting of 3 SSRR and 3 EDR devices. EDR disks are shown in green and SRR rings in gray. The gaps in the SSRR rings are 1mm, and there is a 1 mm gap at the top of each EDR post. The non-Foster elements are modeled in these gaps in the SSRR and EDR devices.

upon the top face of the upper disk equals the current in the post plus the the time derivative of total electric flux departing the bottom face of the top disk [9]:

$$i_p + \frac{d}{dt}\Psi_F = \frac{d}{dt}\Psi_T \ , \tag{10}$$

where i_p is the current in the post, Ψ_T is the total electric flux in coulombs impinging upon the top face of the upper disk of the EDR from sources external to the unit cell, and Ψ_F is the total electric flux that couples between the upper and lower EDR disks (i.e., internal to the unit cell). The left side of (10) then represents the total current (both circuit current and displacement current) flowing from the top disk to the bottom disk, and the right side represents the total displacement current coming from sources external to the unit cell and impinging on the top disk of the EDR.

As noted in [9], the internal electric flux Ψ_F can be represented by a capacitance C_F driven by the voltage v_d across the two disks, and the external electric flux Ψ_T can be represented by a capacitance C_0 coupling to the external voltage potential across the unit cell $v_0 = E_0 l_y$, where $E_0\hat{\mathbf{y}}$ is the incident electric field. Then, (10) becomes:

$$i_p = \frac{d}{dt}\left(v_0 C_0 - \Psi_F\right) = \frac{d}{dt}\left(v_0 C_0 - v_d C_F\right) \ , \tag{11}$$

where capacitance C_F can also be thought of as a leakage capacitance or fringe capacitance around the post inductance.

The voltage between the two disks also equals the voltage across the inductive post, so:

$$v_d = L_p \frac{di_p}{dt} = L_p \frac{d^2}{dt^2}\left(v_0 C_0 - v_d C_F\right) \ , \tag{12}$$

where v_d is the voltage from the top disk to the bottom disk as before, and L_p is the inductance of the metal post connecting the two disks. Taking the Laplace transform results in

$$v_d = s^2 L_p \left(v_0 C_0 - v_d C_F\right). \tag{13}$$

Solving for the voltage v_d then gives

$$v_d = v_0 \frac{s^2 L_p C_0}{1 + s^2 L_p C_F} \ . \tag{14}$$

Next, consider replacing the inductive post L_p with a positive capacitance C_p with reactance $X_p = -j/(\omega C_p)$. The current i_p then flows through this capacitance and the voltage v_d now appears across this capacitance, so:

$$v_d = \frac{1}{C_p}\int i_p\, dt = \frac{1}{C_p}\int \frac{d}{dt}\left(v_0 C_0 - v_d C_F\right)\, dt. \tag{15}$$

after substituting for i_p from (11). Simplifying and solving for v_d results in

$$v_d = \frac{1}{C_p}\left(v_0 C_0 - v_d C_F\right) = v_0 \frac{C_0}{C_p + C_F} \ . \tag{16}$$

Comparing (16) with (14), note that the voltage v_d in (16) *no longer depends on frequency* when the post inductance L_p is replaced by C_p, thus allowing wideband behavior.

The charge on the disks then gives rise to an electric dipole moment:

$$\mathbf{p} = q l_p \ \hat{\mathbf{y}} = v_d C_p l_p \ \hat{\mathbf{y}} = v_0 C_0 l_p \frac{C_p}{C_p + C_F} \ \hat{\mathbf{y}} \ . \tag{17}$$

where $\pm q$ is the charge in coulombs on the disks, $\mathbf{p}$ is the electric dipole moment in the same direction as the applied field $E_0\hat{\mathbf{y}}$, and l_p is the distance between the two disks. In (17), the charge on the bottom disk is $q = \int i_p\, dt$ and

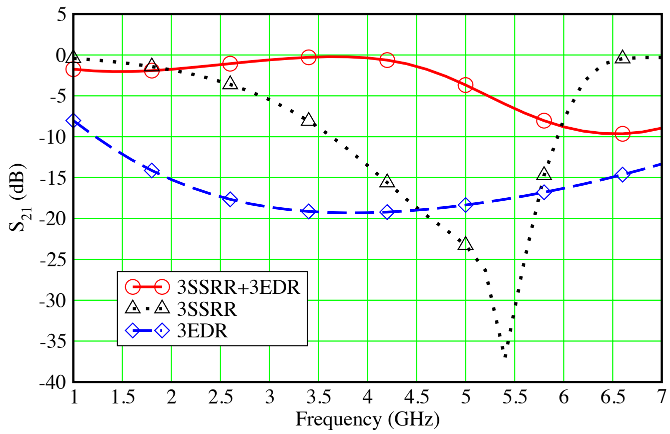

Fig. 4. Simulation results. The solid red curve with circles shows $|S_{21}|$ in dB for the entire structure of Fig. 3. For comparison, the simulated $|S_{21}|$ of only the three EDR structures with negative permittivity is shown in the dashed blue curve with diamonds, and the simulated $|S_{21}|$ of only three SSRR structures with negative permeability is shown in the dotted black lines with triangles.

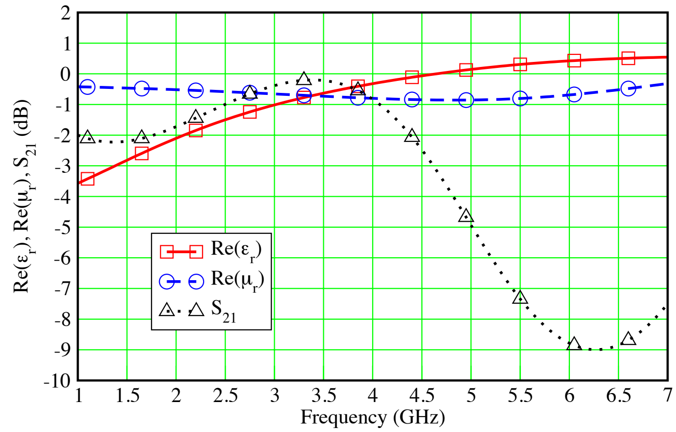

Fig. 5. Extracted values of the real parts of μ_r and ϵ_r for the three unit cell structure shown in Fig. 3. The effective permittivity is shown in the solid red curve with squares and the effective permeability is shown in the dashed blue curve with circles, both on a linear scale. For reference, the magnitude of S_{21} in dB is also shown in the dotted black curve with triangles.

$v_d = (1/C_p)\int i_p\,dt$, so $q = v_d C_p$. Then, polarization $\mathbf{P}$ equals electric dipole moment per unit volume:

$$\mathbf{P} = \frac{\mathbf{p}}{l_x l_y l_z} = E_0 \frac{C_0\, l_p}{l_x l_z}\left(\frac{C_p}{C_p + C_F}\right)\hat{\mathbf{y}}\,. \tag{18}$$

after subtituting $E_0 l_y = v_0$, and for simplicity omitting mixing effects noted in [13]. With $\mathbf{P} = \chi_e \epsilon_\circ \mathbf{E}$ and $\epsilon_r = 1 + \chi_e$, the relative permittivity ϵ_r is

$$\epsilon_r = 1 + \frac{C_0\, l_p}{\epsilon_\circ\, l_x l_z}\left(\frac{C_p}{C_p + C_F}\right), \tag{19}$$

where χ_e is the electric susceptibility, ϵ_r is the effective relative permittivity of the metamaterial, and $\epsilon_\circ = 8.85\times10^{-12}$ F/m is the permittivity of free space.

Therefore, the effective relative permittivity ϵ_r of the EDR in (19) does not vary with frequency, just as there was no frequency dependence in μ_r for the SSRR result of (9) . The effective permittivity ϵ_r becomes a large negative value if C_p is chosen to be negative such that the denominator has $C_p + C_F \approx 0$ and $C_p + C_F > 0$. *Thus, a negative capacitor load replacing the post of an EDR can provide wideband negative effective permittivity.* The desired condition $C_p + C_F > 0$ has the same form as a parallel combination of a negative capacitor with a positive capacitor whose resulting capacitance remains positive [14]. Non-Foster circuits such as a negative capacitor can be designed using negative impedance converters, where recent progress has been made in potential stability issues [14], [15]. Furthermore, in some applications metamaterials do not necessarily need to exhibit negative permittivity and permeability, since devices with non-negative refractive index less than unity or near zero can also be useful.

IV. Simulation Results

The wideband double-negative metamaterial test structure shown in Fig. 3 was chosen to illustrate the performance of the proposed design. The structure consists of three unit cells within a parallel-plate waveguide with perfect electric conductor top and bottom walls separated by $h = 10$ mm, and perfect magnetic conductor side walls separated by $w = 8$ mm. The separation between unit cells was $d = 8$ mm. The SSRR had a radius of 3.2 mm with a 1 mm gap, and the EDR was comprised of two disks 7 mm apart with 3.2 mm radius and a connecting post of 0.15 mm radius. The EDR and SSRR were centered within the waveguide, with 1 mm space between the EDR post and SSRR ring. Each EDR has a 1 mm gap in its post with a negative capacitance of $C_p = -240$ fF placed in the gap. Each SSRR has a 1 mm gap in its ring with a negative inductance of $L_p = -10$ nH placed in the gap. In addition, a negative capacitance of -45 fF was placed in parallel to L_p to compensate for stray capacitance in the ring to help improve bandwidth.

The structure of Fig. 3 was tested in the HFSS 3D electromagnetic simulator. Fig. 4 shows the simulation results for S_{21} for three cases. The solid red curve with circles in Fig. 4 shows $|S_{21}|$ in dB for the entire structure of Fig. 3, and shows wideband double-negative behavior with less than 2 dB loss from 1.0 to 4.5 GHz. The dotted black curve with triangles shows $|S_{21}|$ for the three SSRR devices, with the three EDR devices removed. In the dotted black curve, the insertion loss is due to the negative permeability of the three SSRR devices alone. The dashed blue curve with diamonds shows $|S_{21}|$ for the three EDR devices, with the three SSRR devices removed. In the dashed blue curve, the insertion loss is due to the negative permittivity of the three EDR devices alone.

The effective permeability and effective permittivity of the three unit cell structure of Fig. 3 were extracted from the S-parameters of Fig. 4, drawing upon common methods such as outlined in [17] and [18]. Fig. 5 shows the real part of the effective permittivity (solid red curve with squares) and the real part of the effective permeability (dashed blue curve with circles), both on a linear scale. The dotted black curve with triangles shows $|S_{21}|$ in dB for reference. Note that both the permittivity ϵ_r and permeability μ_r remain negative from 1.0 to 4.5 GHz. Near 1 GHz, ϵ_r approaches -3.5 while μ_r approaches -0.3. Near 5 GHz, ϵ_r becomes positive while μ_r remains negative, suggesting an evanescent non-propagating condition above 4.5 GHz. Also, the attenuation greatly increases above 5 GHz as would be expected when ϵ_r becomes positive while μ_r remains negative.

V. Conclusion

Analysis and simulation results for the proposed non-Foster metamaterial confirm wideband double-negative behavior. Effective permittivity and permeability were extracted from S-parameters and confirm simultaneous negative permittivity and negative permeability from 1.0 to 4.5 GHz.

Acknowledgment

This material is based upon work supported by the National Science Foundation under Grant No. ECCS-1101939.

References

[1] D. R. Smith, W. J. Padilla, D. C. Vier, S. C. Nemat-Nasser *et al.*, "Composite medium with simultaneously negative permeability and permittivity," *Phys. Rev. Lett.*, vol. 84, no. 18, pp. 4184–4187, May 2000.

[2] J. B. Pendry, A. J. Holden, W. J. Stewart, and I. Youngs, "Extremely low frequency plasmons in metallic mesostructures," *Phys. Rev. Lett.*, vol. 76, no. 25, pp. 4773–4776, Jun. 1996.

[3] A. Alù and N. Engheta, "Cloaking a receiving antenna or a sensor with plasmonic metamaterials," *Metamaterials*, vol. 4, no. 2-3, pp. 153–159, 2010.

[4] A. Lai, T. Itoh, and C. Caloz, "Composite right/left-handed transmission line metamaterials," *IEEE Microw. Mag.*, vol. 5, no. 3, pp. 34–50, Sep. 2004.

[5] V. Veselago, "The electrodynamics of substances with simultaneously negative values of epsilon and mu," *Sov. Phys. Usp.*, vol. 10, pp. 509–514, 1968.

[6] S. Tretyakov, "Meta-materials with wideband negative permittivity and permeability," *Microw. Opt. Technol. Lett.*, vol. 31, no. 3, pp. 163–165, 2001.

[7] S. Hrabar, I. Krois, I. Bonic, and A. Kiricenko, "Non-Foster elements - new path towards broadband ENZ and MNZ metamaterials," in *Antennas and Propagation (EUCAP), Proceedings of the 5th European Conference on*, Apr. 2011, pp. 2674–2677.

[8] D.-J. Kim and J.-H. Lee, "Broadband left-handed waveguide with double L-shaped short stubs and E-plane posts," in *Antennas and Propagation (APSURSI), 2011 IEEE International Symposium on*, Jul. 2011, pp. 2958–2960.

[9] T. Weldon, R. Adams, and R. Mulagada, "A novel unit cell and analysis for epsilon negative metamaterial," in *Southeastcon, 2011 Proceedings of IEEE*, Mar. 2011, pp. 211–214.

[10] R. Ziolkowski, "Design, fabrication, and testing of double negative metamaterials," *IEEE Trans. Antennas Propag.*, vol. 51, no. 7, pp. 1516–1529, Jul. 2003.

[11] A. Saha and M. Charise, "Effective permittivity of artificial material composed of metal particles -a generalized picture," in *Southeastcon, 2011 Proceedings of IEEE*, Mar. 2011, pp. 215–219.

[12] J. Pendry, A. Holden, D. Robbins, and W. Stewart, "Magnetism from conductors and enhanced nonlinear phenomena," *IEEE Trans. Microw. Theory Tech.*, vol. 47, no. 11, pp. 2075–2084, Nov. 1999.

[13] K. Rozanov, M. Koledintseva, and J. Drewniak, "A new mixing rule for predicting of frequency-dependent material parameters of composites," in *Electromagnetic Theory (EMTS), 2010 URSI International Symposium on*, Aug. 2010, pp. 584–587.

[14] E. Ugarte-Muñoz, S. Hrabar, and D. Segovia-Vargas, "Investigation of stability of negative impedances for use in active metamaterials and antennas," in *Antennas and Propagation (EUCAP), Proceedings of the 5th European Conference on*, Apr. 2011, pp. 2059–2063.

[15] K. Z. Rajab, Y. Hao, D. Bao, C. G. Parini *et al.*, "Stability of active magnetoinductive metamaterials," *Journal of Applied Physics*, vol. 108, no. 5, pp. 054 904–1–6, 2010.

[16] G. Donzelli, A. Vallecchi, F. Capolino, and A. Schuchinsky, "Metamaterial made of paired planar conductors: Particle resonances, phenomena and properties," *Metamaterials*, vol. 3, no. 1, pp. 10–27, 2009.

[17] J. Barroso and U. Hasar, "Resolving phase ambiguity in the inverse problem of transmission/reflection measurement methods," *Journal of Infrared, Millimeter and Terahertz Waves*, vol. 32, pp. 857–866, 2011.

[18] Z. Szabó and, G.-H. Park, R. Hedge, and E.-P. Li, "A unique extraction of metamaterial parameters based on kramers-kronig relationship," *IEEE Trans. Microw. Theory Tech.*, vol. 58, no. 10, pp. 2646–2653, Oct. 2010.